

PARAMETRISING FLAT-FOLDABLE SURFACES WITH INCOMPLETE DATA

DI QIU*, KA-CHUN LAM†, AND LOK-MING LUI‡

Abstract. We propose a novel way of computing surface folding maps via solving a linear PDE. This framework is a generalization to the existing quasiconformal methods and allows manipulation of the geometry of folding. Moreover, the crucial quantity that characterizes the geometry occurs as the coefficient of the equation, namely the Beltrami coefficient. This allows us to solve an inverse problem of parametrizing the folded surface given only partial data but with known folding topology. Various interesting applications such as fold sculpting on 3D models and self-occlusion reasoning are demonstrated to show the effectiveness of our method.

Key words. Beltrami equation, mathematical origami, fold modelling, self-occlusion reasoning

AMS subject classifications. 65D18, 68U05, 65D17

1. Introduction. Modelling the folding phenomena of surfaces, as well as the study of its regular patterns such as mathematical origami, has attracted lots of interests in computer graphics and mathematics. In this paper we propose to model and study such phenomena from the geometric partial differential equations (PDEs) point of view. The key equation is the so-called *alternating Beltrami equation*

$$\frac{\partial f}{\partial \bar{z}}(z) = \mu(z) \frac{\partial f}{\partial z}(z), \quad z \in \Omega$$

where Ω is a bounded domain with regular boundary. The point is that here the *Beltrami coefficient* μ is allowed to take values in the Riemann sphere, in contrast to the ordinary Beltrami equation which requires the Beltrami coefficient to be strictly inside the unit disk.

There are many advantages to model and study the surface folding with alternating Beltrami equation. One of the most prominent reasons is its connection to quasiconformal geometry, where the Beltrami coefficient can be used to encode the *conformal distortion* of the mapping. In particular, it can be used to control the folding and unfolding of the mapping. But it must be noted that the solution mapping of the alternating Beltrami equation is not orientation-preserving in general, and so the traditional notion of conformal distortion has to be extended. This is explained in Section 2 below.

1.1. Problem description. Solving Beltrami equations has been a central component in computational quasiconformal geometry, which has many successful applications to medical imaging etc [17, 19]. However, it turned out that the previous method¹ for solving ordinary Beltrami equation could no longer be applied in our setting, as is illustrated in Figure 1, where the correct alternating Beltrami coefficient is used. This is even more so for the modelling task, where the boundary condition is usually not known *a priori*. The reason for the failure is that the folding or unfolding map is genuinely different inside and outside the folded region, corresponding to $|\mu| > 1$ and $|\mu| < 1$ respectively. This demonstrates the challenging task of numeri-

*Department of Mathematics, The Chinese University of Hong Kong. dqiu@math.cuhk.edu.hk.

†Department of Computing + Mathematical science, California Institute of Technology. kclam@caltech.edu.

‡Department of Mathematics, The Chinese University of Hong Kong. lmhui@math.cuhk.edu.hk.

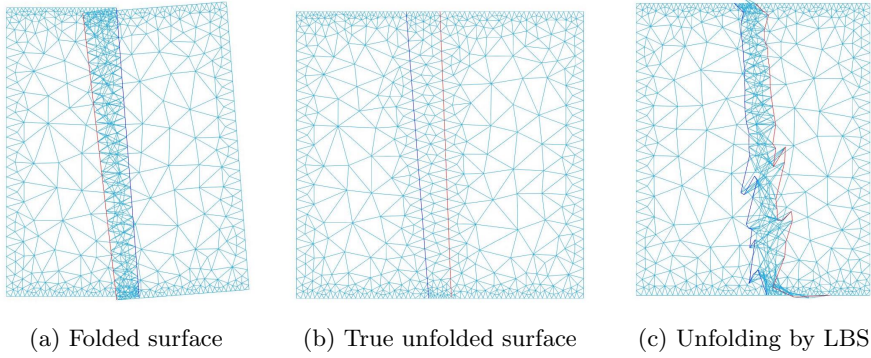


Fig. 1: The previous method fails to compute the correct unfolding map

cally solving alternating Beltrami equation.

In applications involving folded surface, one of the fundamental problem is that when only one perspective of the surface is given, it is often *self-occluded*. This corresponds to the situation where the data needed to solve for the desired solution of the alternating Beltrami equation is often incomplete by a large portion. In other words, we have an *inverse problem* of inferring the geometric missing data in order to parametrize the self-occluded surface.

1.2. Contributions of this paper. Our work can be considered as the first application of quasiconformal methods to the problem of modelling and studying the folding phenomena. The main contributions include our methods to attack the two problems described above, which we describe in more details below.

1.2.1. Numerically solving alternating Beltrami equation. We found out that the failure of the previous method for solving alternating Beltrami equation is that it does not take care of the fact that the real and imaginary parts of the solution are *coupled* in a very strong way. This can be understood as in the classical case that the real and imaginary parts of a conformal mapping (i.e. holomorphic function) on the unit disk are related by the Hilbert transform. In our method this coupling is realized in the proposed **generalized quasiconformal energy** defined in Definition 2.6 below. The numerical method is derived from the proposed energy, works for bounded domains with arbitrary topology and amounts to simply solving a sparse linear system.

This variational formulation in fact has an interesting discrete geometric interpretation: it is a quadratic cost of gluing “ μ -altered” mesh triangles together to form the discrete solution surface. This in fact is related to the *as similar as possible* algorithm proposed by Igarashi et al [14], which is related to various famous algorithms that promote the rigidity of the mapping [24, 23]. While we must note that these type of energies need not arise from the discretization of a smooth energy (or equivalently differential operator). In the setting of [14], we found that for each mesh triangle our energy differs from theirs by a nonlinear factor depending on the mesh condition.

¹In the previous method, the ordinary Beltrami equation is transformed into a system of elliptic equations, where the ellipticity of the PDEs comes from the condition that $|\mu| < 1$.

This is explained in Section 2.3.3. It is also worth remarking that more sophisticated algorithms such as the *as-rigid-as-possible* algorithm in [23] can be regarded as a prior on the Beltrami coefficients.

1.2.2. Parametrizing flat-foldable surfaces with incomplete data. To tackle the challenge of incomplete data, one must exploit the structure of the problem and design suitable optimization algorithms thereof. We will mainly focus on the problem for *flat-foldable* surfaces, informally known as *planar origamis*. This is due to the following two reasons:

1. Finding a desirable parametrization can be formulated as an optimisation problem of minimizing the conformal distortion of the proposal mapping for parametrization.
2. It is where our framework of using alternating Beltrami equation is most effective, since other, especially three dimensional geometric feature of the folded surface, such as mean curvature, does not belong to our framework but can be tackled by pre- or post-processing.

To solve this ill-posed inverse problem, we propose the “**Reinforcement Iteration**” algorithm. The algorithm starts with a initial domain with the *singular set configuration* of the same topological type with the target surface, and then iteratively find the domain that will result in smaller conformal distortion. So alternatively, one can view the problem as finding a desirable Beltrami coefficients of the mapping from the initial domain and the desirable target surface, that is a coefficient problem for the alternating Beltrami equation. Empirically our algorithm converges at about the rate $O(1/N)$, see Figure 4. We shall layout more details in Section 3.4.

1.3. Related work. Here we briefly list some important related work in this area, while they are by no means an exhaustive survey.

Computational quasiconformal geometry. Computations of conformal mapping [18, 9] turned out to be very useful in computer graphics. Since the seminal work of Gu and Yau [11], the conformal geometry framework in surface registration tasks has advanced significantly. Earlier work generalizing these ideas is already implicit in the work of Seidel [28]. The quasiconformal extension of this framework was proposed by Lui and his coauthors [20, 19, 4], with successful applications to medical image registration and surface registration. The quasiconformal method is able to handle large deformations, where conformal methods typically fails. Our work is an extension along this line, allowing the manipulation of folding, which opens up a new area to be explored.

Modelling the folding phenomena and mathematical origamis. In computer graphics there has been a lot of work on modelling the folding phenomena of surfaces. Many interesting works focus on 3D interactive design. These include the method of thin plate form with explicit user control of folding angles for interactive 3D graphics design in [29], which can also achieve the sharp folding edges as we do here. Our framework and techniques are completely different, especially here the we are taking advantage of the fact that alternating Beltrami equation can be solved effectively in 2D. On the other hand, there are studies of developable surface design with curved folding [15], taking the advantage of the special quad meshes, while we don’t have this restriction. There are also applications in such as the 4D printing of [16] and material design in [10]. Finally, we must mention the work of Demaine and Tachi [8], who developed algorithms to fold a planar paper into arbitrary 3D shapes. We expect to discover interesting connections to them in the future work.

2. The alternating Beltrami equation and its computational framework. As alluded in the introduction above, we shall be setting our computational framework within the quasiconformal theory, most notably the *Beltrami equation*:

$$\frac{\partial f}{\partial \bar{z}}(z) = \mu(z) \frac{\partial f}{\partial z}(z),$$

satisfied by continuously differentiable quasiconformal mappings f defined on some domain $\Omega \subset \mathbb{C}$, and also valid if it is interpreted in the weak sense. Traditionally, this equation has been studied in the case where the *complex dilatation*, or *Beltrami coefficient* $\|\mu\|_\infty < 1$, and was shown, for simply connected domains which are not the whole plane, that there is a one-one correspondence between the measurable Beltrami coefficients satisfying the bound and the quasiconformal homeomorphisms, up to some normalization. This is the well known *Measurable Riemann mapping theorem*.

Since we are studying the folding phenomena of a continuous mapping, where rigorously speaking it is not a homeomorphism in the conventional sense, the equation here will be somewhat different, but as an extension of the above. More precisely, such folding phenomena will be corresponding to the case $|\mu| > 1$ in certain distinguished subset of the domain. The extended version of the Beltrami equation, is sometimes called the *alternating Beltrami equation*, and was first studied by Uri Srebro [25].

To get a better idea of the alternating Beltrami equations, and why the folding phenomenon occurs for the solutions of these equations, we illustrate it with the effect of the Beltrami coefficients on a single triangle (i.e. the linearized effect at the tangent space level). This should provide one with geometric intuition for the solutions on a triangulated mesh.

2.1. The effect of Beltrami coefficient on a single triangle. Let us rewrite the Beltrami equation as a system of first-order PDEs in the usual Cartesian coordinate. Suppose $f : (x, y) \mapsto (u, v)$ satisfies the equation $\frac{\partial f}{\partial \bar{z}}(z) = \mu(z) \frac{\partial f}{\partial z}(z)$. If we write $\mu = \rho + i\tau$, $\frac{\partial f}{\partial \bar{z}} = (u_x - v_y) + i(u_y + v_x)$ and $\frac{\partial f}{\partial z} = (u_x + v_y) + i(-u_y + v_x)$, then it's not hard to see that

$$(1) \quad \begin{bmatrix} u_y \\ v_y \end{bmatrix} = \frac{1}{(1+\rho)^2 + \tau^2} \begin{bmatrix} 2\tau & |\mu|^2 - 1 \\ 1 - |\mu|^2 & 2\tau \end{bmatrix} \begin{bmatrix} u_x \\ v_x \end{bmatrix},$$

here we have assumed $\rho \neq -1$ and $\tau \neq 0$.

Hence for a single triangle, on which we assume f is linear, the mapping is determined up to a similarity transform (uniform scaling and rotation) in the target domain. Now suppose f maps a domain triangle $[v_1, v_2, v_3] = [(0, 0), (1, 0), (x, y)]$ to the target triangle $[w_1, w_2, w_3] = [(0, 0), (1, 0), (u(x, y), v(x, y))]$. Then

$$(2) \quad \begin{bmatrix} u(x, y) \\ v(x, y) \end{bmatrix} = \begin{bmatrix} 1 & \frac{2\tau}{(1+\rho)^2 + \tau^2} \\ 0 & \frac{1 - |\mu|^2}{(1+\rho)^2 + \tau^2} \end{bmatrix} \begin{bmatrix} x \\ y \end{bmatrix}.$$

One can check that the set of points for the family of μ with each fixed modulus $|\mu| \neq 1$ form a circle, whereas in the case $|\mu| = 1$ the circle degenerates to the x -axis.

Of course, in the equation (1) one can go beyond to $|\mu| > 1$, where the anti-diagonal terms experience a change of sign, leading to a “flipping” of the triangle. In

fact, for a single triangle, everything remains the same after an mirror reflection about the x -axis, and the case $|\mu| = \infty$ corresponds to the *anti-conformality* of the mapping. What is more, for each fixed argument $\arg(\mu)$ and let the modulus $|\mu|$ vary, the set of solution points form an arc of a circle, passing through the points (x, y) and $(x, -y)$. Altogether, we see that the Beltrami coefficients in effect form a bipolar coordinate in the plane containing the target triangle. Therefore, it describes all possible angular distortion at the tangent space level, including those having a change of orientation.

2.2. Definitions of folding homeomorphism, singular set configuration and flat-foldability. In this section we give the mathematical definitions related to the folding phenomena we are studying. For a more thorough treatment, readers can refer to Gutlyanskii et al [13].

DEFINITION 2.1 (Folding homeomorphism and its singular set configuration). *Let X and Y be oriented surfaces. A continuous, discrete mapping f (discrete means $f^{-1}(y)$ are isolated in X for all $y \in Y$) is called a folding homeomorphism if there is a subset $\Sigma \subset X$, of Hausdorff dimension 1, with (X, Σ) forming a locally finite two color (white and black) map, such that when restricting to the connected components of the white (or black) region, f is an orientation preserving (or respectively, reversing) homeomorphism. The pair (X, Σ) is called the singular set configuration of f , and is sometimes simply referred to as Σ if it is clear from the context.*

The white and black region are often denoted as X_Σ^+ and X_Σ^- respectively, or simply X^+ and X^- if Σ is clear from the context. And on X^+ the folding homeomorphism f is orientation preserving, and X^- the orientation reversing part.

Sometimes we would also like to give names to the points in the singular set according to the properties of f . The definition below suffices for our purposes, but they are by no means exhaustive.

DEFINITION 2.2 (Folding point and cusp point). *Let $f : X \rightarrow Y$ be a folding homeomorphism with singular set configuration Σ .*

- *A point $p \in \Sigma$ is called a folding point if there is an open neighborhood U of p such that $U \setminus \Sigma$ is disconnected into exactly 2 simply connected components, and the restriction $f|_U$ is topologically equivalent to $(x, y) \mapsto (x, |y|)$, where $U \cap \Sigma$ plays the role of x -axis.*
- *A point $p \in \Sigma$ is called a cusp point if there is an open neighborhood U of p such that $U \setminus \Sigma$ is disconnected into exactly $2n$ simply connected components, $n > 1$, and the remaining points $p' \in (\Sigma \cap U) \setminus \{p\}$ are all folding points.*
- *The collection of paths in Σ consisting of all folding points is called folding lines.*

We illustrate these concepts with the famous paper crane origami, in Figure 2, where for better visualization we use yellow and purple instead of white and black.

Next we give a more analytic definition for the folding homeomorphism, which is the subject of our computational framework.

DEFINITION 2.3. *A generalized K -quasiconformal mapping $f : \Omega \subset \mathbb{C} \rightarrow \mathbb{C}$, $K \geq 1$ with singular configuration Σ is a solution of some alternating Beltrami equation $\frac{\partial f}{\partial \bar{z}}(z) = \mu(z) \frac{\partial f}{\partial z}(z)$, such that in Ω^+ and Ω^- it holds that $|\mu| < 1$ and $|\mu| > 1$,*

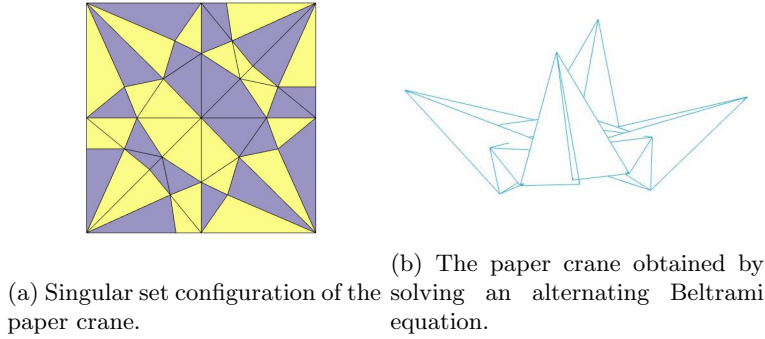


Fig. 2: The paper crane origami

respectively, and satisfy the bound

$$-K \leq \frac{1 + |\mu(z)|}{1 - |\mu(z)|} \leq K$$

for all $z \in \Omega$ except for a set of Lebesgue measure zero.

For example, any planar origami will correspond to such a generalized K -quasiconformal mapping with $K = 1$, in which case it will be called generalized conformal.

Notice also that when the paper is rigidly folded, the folding lines of the singular set configuration are all Euclidean geodesics, reflecting the rigidity nature of the piece of paper. Such rigidity is also manifested via a well-known condition about how folding lines join each other at a cusp point, which we define below.

DEFINITION 2.4 (Flat-foldability). *Let $n > 1$ be an integer and suppose there are $2n$ Euclidean geodesics emanating from a cusp point $p \in U \subset \mathbb{C}$. Then the neighborhood U is said to be flat-foldable if the alternating sum of the angles $(\alpha_i)_{i=1}^{2n}$ formed by every two neighboring Euclidean geodesics satisfy the condition*

$$\sum_{i=1}^{2n} (-1)^i \alpha_i = 0.$$

This condition is also known as the *Kawasaki's condition* [6] for flat-foldable surfaces. It is only a necessary condition for a more physical definition of flat-foldability, since it does not eliminate the case when the surface interpenetrates itself. Since we are working in 2D, this issue is not so important. The flat-foldability is one important criterion for generating synthetic data, but otherwise will not play a significant role in the optimization algorithm we propose.

2.3. The numerical method for solving alternating Beltrami equations.

Before arriving at the our proposed framework of computing alternating Beltrami equations, we shall begin by looking into the existing method. This should shed light on the structure of the solution and eventually lead to the correct framework.

2.3.1. The decoupling method and the necessary condition. Perhaps the most straightforward way to solve the Beltrami equation is to decouple the corresponding first order system into two independent second order equations, namely,

PROPOSITION 2.5 (Necessary condition). *Suppose for $z \in \Omega \setminus \Sigma$, $f(z) = u(z) + iv(z)$ satisfies the equation $\frac{\partial f}{\partial \bar{z}}(z) = \mu(z) \frac{\partial f}{\partial z}(z)$. Assume the domain Ω is given the usual Euclidean geometry, and $|\mu| \neq 1$, then we have*

$$(3) \quad \begin{cases} -\nabla \cdot (A \nabla u(z)) &= 0 \\ -\nabla \cdot (A \nabla v(z)) &= 0 \end{cases}$$

where $A = \frac{1}{1-|\mu|^2} \begin{bmatrix} (\rho-1)^2 + \tau^2 & -2\tau \\ -2\tau & (1+\rho)^2 + \tau^2 \end{bmatrix}$, and $\mu = \rho + i\tau$.

Proof. Observe that $\frac{\partial f}{\partial \bar{z}}(z) = \mu(z) \frac{\partial f}{\partial z}(z)$ can be transformed into

$$\begin{bmatrix} u_x \\ u_y \end{bmatrix} = \begin{bmatrix} 0 & 1 \\ -1 & 0 \end{bmatrix} A \begin{bmatrix} v_x \\ v_y \end{bmatrix}.$$

Then making use of the commutativity of second order partial derivatives $u_{xy} = u_{yx}$ under the Euclidean metric, we obtain

$$\nabla \cdot (A \nabla u(z)) = 0.$$

The other equation is obtained in a similar way. \square

Note that the coefficient matrix A is positive (or negative) definite if $|\mu| < 1$ (or $|\mu| > 1$, respectively). If U is any open neighborhood, on which A is either positive or negative but not both, then it is not hard to see that they are the Euler-Lagrange equations of the modified Dirichlet energies

$$(4) \quad E_{\tilde{A}}(u; U) = \frac{1}{2} \int_U \|\tilde{A}^{1/2} \nabla u\|^2 dx dy, \quad E_{\tilde{A}}(v; U) = \frac{1}{2} \int_U \|\tilde{A}^{1/2} \nabla v\|^2 dx dy,$$

where \tilde{A} denotes A if it is positive definite, or $-A$ if negative definite. Therefore, we see that in general the global variational problem must be separated according to whether $|\mu| < 1$ or $|\mu| > 1$ in the domain Ω . We shall often denote Ω^+ (or Ω^-) to be the largest open subset such that $|\mu| < 1$ (or $|\mu| > 1$, respectively).

The derived system (3) is a **necessary condition** that in principle should be satisfied by any other method which respects the Euclidean geometry of Ω . By this decoupling, u and v can be solved independently. But in order for the solution pair (u, v) to make sense as a quasiconformal mapping, the two associated equations must be provided with the correct boundary values. Such a requirement is often too strong, and at the same time completely ignores the rigidity properties of these mappings that one may take advantage of (as one can see from the measurable Riemann mapping theorem, these mapping has certain rigidity similar to those of holomorphic functions). This is undesirable since the entire set of boundary data are not available in our problem. To circumvent this we have to consider a method that takes into account the coupled nature of u and v .

2.3.2. Generalized quasiconformal energy. Our approach takes inspiration from the well-known *least square conformal energy*, studied in [18, 9], which take into account the coupling of u and v . Its continuous formulation is

$$\int_{\Omega} \left\| \frac{\partial f}{\partial \bar{z}} \right\|^2 dx dy,$$

which is equivalent to

$$\int_{\Omega} \left\| \nabla u + \begin{bmatrix} 0 & -1 \\ 1 & 0 \end{bmatrix} \nabla v \right\|^2 dx dy.$$

The corresponding matrix associated to its discretization is the well-known *cotangent weight* matrix minus a certain “area matrix” [21, 9]. This area matrix in fact plays the role of certain Neumann boundary condition. One would expect analogous results to hold in the quasiconformal setting.

But in the quasiconformal case, it is not an entirely trivial matter to formulate the correct analog. For example, one can formulate arbitrary quadratic energies in such a way that $\int_{\Omega} F(\frac{\partial f}{\partial \bar{z}}, \mu, \frac{\partial f}{\partial z}) dx dy$ where F is a quadratic cost functional such that $F(\cdot) = 0$ if $\frac{\partial f}{\partial \bar{z}} = \mu \frac{\partial f}{\partial z}$. This formulation includes for example $\int_{\Omega} \left\| \nabla u + \begin{bmatrix} 0 & -1 \\ 1 & 0 \end{bmatrix} A \nabla v \right\|^2 dx dy$, etc.

However, among these energies, there is essentially only one (i.e. modulo change of variable and multiplying by a positive constant) that will give rise to the necessary condition we obtained earlier.

DEFINITION 2.6. *The **generalized quasiconformal energy** with Beltrami coefficient μ of the mapping $z = (x, y) \mapsto (u, v)$ is defined to be*

$$\begin{aligned} E_{LSQC}(u, v; \mu) &= \frac{1}{2} \int_{\Omega^+} \left\| P \nabla u + \begin{bmatrix} 0 & -1 \\ 1 & 0 \end{bmatrix} P \nabla v \right\|^2 dx dy \\ &\quad - \frac{1}{2} \int_{\Omega^-} \left\| P \nabla u + \begin{bmatrix} 0 & -1 \\ 1 & 0 \end{bmatrix} P \nabla v \right\|^2 dx dy \\ &=: E_{LSQC}^+(u, v; \mu) - E_{LSQC}^-(u, v; \mu), \end{aligned}$$

where $\Omega^+ = \text{int} \{z \in \Omega : |\mu(z)| < 1\}$, $\Omega^- = \text{int} \{z \in \Omega : |\mu(z)| > 1\}$, and

$$P = \begin{cases} \frac{1}{\sqrt{1-|\mu|^2}} \begin{bmatrix} 1-\rho & -\tau \\ -\tau & 1+\rho \end{bmatrix} & \text{if } z \in \Omega^+ \\ \frac{1}{\sqrt{-1+|\mu|^2}} \begin{bmatrix} 1-\rho & -\tau \\ -\tau & 1+\rho \end{bmatrix} & \text{if } z \in \Omega^-. \end{cases}$$

Consequently, we have the following identity

$$E_{LSQC}(u, v; \mu) = (E_{\tilde{A}}(u; \Omega^+) + E_{\tilde{A}}(u; \Omega^+)) - (E_{\tilde{A}}(u; \Omega^-) + E_{\tilde{A}}(v; \Omega^-)) - \mathcal{A}(u, v),$$

where $\tilde{A} = P^T P$ is the same matrix described previously in (4), and

$$\mathcal{A}(u, v) := \int_{\Omega^+} (u_y v_x - u_x v_y) dx dy - \int_{\Omega^-} (u_y v_x - u_x v_y) dx dy$$

is the **unsigned** area of the target surface. Observe that if $\Omega^- = \emptyset$ and $\mu \equiv 0$, we easily obtain the classical lower bound of the Dirichlet energy

$$(5) \quad E_{\tilde{A}}(u) + E_{\tilde{A}}(v) \geq \mathcal{A}(u, v).$$

If we assume the domain $\partial\Omega$ has Lipschitz boundary, then the quantity $\mathcal{A}(u, v)$ is equal to the following integral on the boundary

$$\frac{1}{2} \int_{\partial\Omega} (v \nabla u - u \nabla v) \times \nu d\Gamma,$$

where $\nu(z)$ is the outer unit normal vector when $z \in \partial\Omega^+$, and inner unit normal if $z \in \partial\Omega^-$, and $d\Gamma$ is the standard measure of $\partial\Omega$. Actually, the coupling between u and v is realized as certain boundary condition applied to solving (3). The following derivation of the second order equations with boundary condition is standard.

THEOREM 2.7. *Suppose μ is uniformly bounded away from 1, Ω is connected with Lipschitz boundary, and suppose there exists one pair (\tilde{u}, \tilde{v}) , $\tilde{u}, \tilde{v} \in W^{2,2}(\Omega)$, such that*

$$\begin{aligned} E_{LSQC}^+(\tilde{u}, \tilde{v}; \mu) &= \arg \inf_{u, v \in W^{1,2}} E_{LSQC}^+(u, v; \mu), \\ E_{LSQC}^-(\tilde{u}, \tilde{v}; \mu) &= \arg \inf_{u, v \in W^{1,2}} E_{LSQC}^-(u, v; \mu). \end{aligned}$$

Then they satisfy the following Neumann boundary problem

$$(6) \quad \begin{cases} -\nabla \cdot (A\nabla u) = 0 & \text{in } \Omega \\ -\nabla \cdot (A\nabla v) = 0 & \text{in } \Omega \\ \partial_{A\nu} u + \nabla v \times \nu = 0 & \text{on } \partial\Omega \\ \partial_{A\nu} v - \nabla u \times \nu = 0 & \text{on } \partial\Omega \end{cases},$$

where again $\nu(z)$ is the outer unit normal vector when $z \in \partial\Omega^+$, and inner unit normal if $z \in \partial\Omega^-$.

We can observe that the solution is only defined up to post-composition with conformal mappings. Hence there need to be, but only a few, additional constraints in order to obtain a unique solution. We shall now turn to the discrete setting to address this problem.

COROLLARY 2.8. *The $2V \times 2V$ -matrix (up to a nonzero constant scaling) associated to the triangular mesh discretization of the generalized quasiconformal energy is*

$$M := \begin{bmatrix} \mathcal{L}_\mu & 2\mathcal{A} \\ -2\mathcal{A} & \mathcal{L}_\mu \end{bmatrix},$$

when applied to the $2V$ -coordinate vector $[u, v]^T$. Here \mathcal{L}_μ is the cotangent matrix associated to the operator $\nabla \cdot A\nabla$, and $\begin{bmatrix} 0 & 2\mathcal{A} \\ -2\mathcal{A} & 0 \end{bmatrix}$ is the **unsigned** area matrix of the target triangular mesh.

Proof. The $V \times V$ matrix \mathcal{L}_μ corresponds to the discretization of the differential operator $\nabla \cdot (A\nabla)$. The unsigned area matrix has non-zero entries only corresponding to the boundary vertices. It is immediate to check, by examining the corresponding rows of the linear system, that for interior vertices, the solution (u, v) satisfies $-\nabla \cdot (A\nabla u) = 0$ and $-\nabla \cdot (A\nabla v) = 0$, while on the boundary, it satisfies $\partial_{A\nu} u + \nabla v \times \nu = 0$ and $\partial_{A\nu} v - \nabla u \times \nu = 0$ respectively. \square

In order to obtain a non-trivial solution, one has to add at least two linearly independent constraints. This is related to the rank of the cotangent matrix and its rigidity property, studied in [12].

In the next section we shall give a geometric interpretation for the generalized quasiconformal energy as well as the matrix M .

2.3.3. Geometric interpretation for the discretized generalized quasiconformal energy. There is one method that, in our opinion, best suited for explaining the geometric intuition in the discrete formulation. This is what we would

like to call the *As- μ -As Possible ($A\mu AP$)* method for the following reason. It is a variant of Igarashi et al's [14] "as similar as possible -(ASAP)" alternative construction of conformal mappings, which is a representative for a family of mesh editing methods common to the computer graphics community. As we shall later see, it is only suitable for computing the alternating Beltrami equations when the mesh triangles have a least angle lower bound, and/or the Beltrami coefficients away from the degeneracy threshold 1.

The idea can be seen as resulted from a shifted view point about a quasiconformal mapping. In fact, it can be regarded as a conformal mapping between domains with different *conformal structures*. In the case of triangular mesh, this structure can be thought of as the angle triples $(\alpha_1, \alpha_2, \alpha_3)$ of each triangular face of the mesh.

We can describe how Beltrami coefficients alter the discrete conformal structure from Subsection 2.1. As we already knew, the Beltrami coefficient of a piecewise linear mapping f , defined on each triangular face, are encoded entirely via the angles of the corresponding domain and target triangles. Therefore, given a set of Beltrami coefficients $\{\mu_T\}_{T \in \mathcal{T}}$ for each triangle T in the domain mesh \mathcal{T} , we can find for each of them its target triangle $f_{\mu_T}(T)_{\text{loc}}$. These target triangles are defined only up to a similarity transform, thereby are of a local nature. Then one applies Igarashi's ASAP method. Roughly speaking, one looks for a global mapping \tilde{f} that tries to glue these local target triangles together using local transforms that are rotations with uniform scaling.

Let us explain the formulation in more details, following Igarashi et al. The important observation to make for a triangular mesh is that the set of vertices themselves satisfy certain linear relations, if the angles are specified, which ultimately accounts for the coupling of u and v .

Suppose the vertices of the local target triangles $f_{\mu_T}(T)_{\text{loc}}$ are

$$[w_i, w_j, w_k] := [(0, 0), (1, 0), (u_{\mu_T}(x, y), v_{\mu_T}(x, y))],$$

found via the formula (2). We can express the 2D coordinate of any one of the vertex in terms of the other two, in the following way; for example

$$(7) \quad \begin{bmatrix} w_{kx} \\ w_{ky} \end{bmatrix} = \begin{bmatrix} w_{ix} \\ w_{iy} \end{bmatrix} + \begin{bmatrix} a_k & -b_k \\ b_k & a_k \end{bmatrix} \begin{bmatrix} w_{jx} - w_{ix} \\ w_{jy} - w_{iy} \end{bmatrix}$$

and a_k, b_k in this case are easily seen to be

$$a_k = u_{\mu_T}(x, y), \quad b_k = v_{\mu_T}(x, y).$$

Here it is worthwhile to observe how w_x and w_y are coupled in the equation.

Abusing the notation, we still denote the vertices after gluing by $[w_i, w_j, w_k]$. Then (7) suggests the energy obtained by simply summing the quadratic discrepancies

$$(8) \quad \arg \min_w \sum_{T \in \mathcal{T}} \sum_{w_k \in T} \left\| \begin{bmatrix} w_{kx} \\ w_{ky} \end{bmatrix} - \left(\begin{bmatrix} w_{ix} \\ w_{iy} \end{bmatrix} + \begin{bmatrix} a_k & -b_k \\ b_k & a_k \end{bmatrix} \begin{bmatrix} w_{jx} - w_{ix} \\ w_{jy} - w_{iy} \end{bmatrix} \right) \right\|^2,$$

and in order to obtain a non-trivial solution one has to provide at least two linearly independent constraints.

We remark that while this formulation seems natural, it actually fails to satisfy the discretization of the necessary condition in Proposition 2.5. In fact, a straightforward comparison of the $A\mu$ AP energy (7) with the generalized quasiconformal energy yields the following.

COROLLARY 2.9. *For a single μ -altered triangle T with edge lengths (l_1, l_2, l_3) , the $A\mu$ AP matrix is a constant multiple of the LSQC matrix with the constant proportional to*

$$\text{Area}(T) \sum_{i=1}^3 \frac{1}{l_i^2}.$$

In particular, we see that the $A\mu$ AP energy does not handle well the case when the area of a mesh triangle is small, yet its perimeter remains large. This happens when either the assigned angular distortion is large, namely when μ is close to 1, or the original mesh is not well conditioned.

In the sequel, solving an alternating Beltrami equation using the above LSQC method is denoted in operator²form

$$\mathcal{T}' = \text{LSQC}(\mathcal{T}, (\mu_T)_{T \in \mathcal{T}}, \mathcal{C}),$$

where \mathcal{T}' , \mathcal{T} are the computed target triangular mesh and the domain mesh, respectively; $(\mu_T)_{T \in \mathcal{T}}$ is the set of Beltrami coefficients on each face, and \mathcal{C} is the set of constraints.

3. The reinforcement iteration algorithm. In this section we give our proposed solution to the problem of incomplete boundary and singular set data.

3.1. Assumptions for desirable mappings. The first assumption is made with regard to our prior knowledge about the type of the target flat-foldable surface.

ASSUMPTION 3.1. *The domain Ω as a set, and the type of the singular set configuration are given.*

In practice it often means to assume the boundary $\partial\Omega$ has certain shape (e.g. a rectangle), and the singular set as a set of landmark constraints are given.

The second assumption is about the geometric property of the mapping f . Ideally, we would like to have the mapping $f : \Omega \rightarrow S$ is a “generalized isometry”. For example, this will eliminate the cases where the occluded part is too much distorted compared to where it comes from in the domain Ω , as is unlikely the case physically. A relaxation of this assumption can be easily made precise, one that we shall always adopt:

ASSUMPTION 3.2. *The mapping $f : \Omega \rightarrow S$ is generalized conformal.*

We see that this corresponds to the case $K = 1$, a condition that is necessary to rigid deformation but makes the problem much easier to solve. This is in particular the case for discrete surfaces, due to the rigidity property of the Cotangent matrices.

3.2. Occlusion reasoning. For completeness we mention how to obtain the occluded region from the singular set configuration. Let us denote $S^- \subset S$ to be

²The source code is available at <https://github.com/sylqiu/Least-square-beltrami-solver>.

the part that has the back side of the flat-foldable surface facing up, i.e. the region resulted from the reverse of orientation of f . It is clearly possible that some portion of it is included in S_{vis} . The occluded part S_{occ} of S can be partitioned into two categories:

- Folded part: $S^- \cap S_{\text{occ}}$. This portion of the paper goes in under after the sharp crease and happens to be occluded.
- Non-folded part: $S_{\text{occ}} \setminus S^-$. This is the part that is occluded due to the foldover, as well as the perspective of the “camera”, but where f is still orientation preserving.

Due to the above partition, the occluded part S_{occ} can be easily obtained if we know S^- . Indeed, what we see in the picture is a projection in the perspective of the camera

$$\pi : S \rightarrow S_{\text{vis}},$$

when restricted to S_{vis} is simply the identity map

$$\pi|_{S_{\text{vis}}} \equiv id.$$

Now suppose we know where the paper is folded in S . Then the non-folded occluded part can be found simply by

$$S_{\text{occ}} \setminus S_{\text{fold}} = \pi^{-1}(S_{\text{fold}} \cap S_{\text{vis}}) \setminus (S_{\text{vis}} \cup S_{\text{fold}}).$$

For example, the occluded part of the above is shown in Figure 13, found via the above approach.

3.3. The idea of the reinforcement iteration. Let us first consider the case where the entire boundary and singular set of the folded surface S is given, for example, the one shown in Figure ... In order to parametrize S , one needs to start with some initial singular set configuration, like the one in Figure ... We can easily construct a mapping $g : \Omega_{\Sigma_0} \rightarrow S$ by enforcing all the constraints.

In general, g will not be a conformal mapping, as the initial singular set configuration may not coincide with the reality. So instead, there exists a quasiconformal mapping

$$\varphi : \Omega_{\Sigma_0} \rightarrow \Omega_{\Sigma}$$

that maps the initial configuration to the correct one. Its relation with the desired generalized conformal mapping f can be observed as a commutative diagram below

$$(9) \quad \begin{array}{ccc} \Omega_{\Sigma_0} & \xrightarrow{\varphi} & \Omega_{\Sigma} \\ \downarrow g & \swarrow f & \\ S & & \end{array}$$

In this case, once we obtain the folded surface S from the mapping g , since the entire boundary and singular set data is given, the generalized conformal “unfolding homeomorphism” $h = f^{-1}$ can be constructed by solving the alternating Beltrami equation

$$(10) \quad \begin{cases} \frac{\partial}{\partial \bar{z}} h &= 0 \text{ in } S^+ \\ \frac{\partial}{\partial z} h &= 0 \text{ in } S^- \end{cases}$$

And in this way the mapping φ is obtained by the composition $h \circ g$.

However, when only partial data of S is provided, it is no longer valid to obtain the folded surface S by constructing g in the above manner. In fact, the heart of the matter is that the surface S needs to be defined properly. We shall accept any folded surface S that satisfies the following definition.

DEFINITION 3.3. *Let S_{vis} be a set of partial boundary and singular set data, and Ω_{Σ_0} be the domain with an initial singular set configuration. A folded surface S is called admissible if*

1. *The singular set configuration of S is of the same topological type with the target surface, which is assumed to be known.*
2. *There is a subset $C \subset S$ such that there is a bijective mapping from C to S_{vis} .*
3. *There exist mappings g, φ, f such that f is the solution of the alternating Beltrami equation (10), and the diagram (9) commutes.*

We now proceed to describe the idea of finding some admissible folded surface S by a sequence of folded surfaces S_n , in the following way. Write $\Omega_n = \Omega_{\Sigma_n}$. Let $g_n : \Omega_n \rightarrow S_n$ be a generalized quasiconformal folding homeomorphism that satisfies the constraints

$$f_n|_{\Omega_{vis}} : \Omega_{vis} \rightarrow S_{vis},$$

where $\Omega_{vis} \subset \Omega$ is the corresponding subset corresponding to the partial boundary and singular set data. Let $h_n : S_n \rightarrow \Omega_n$ be “unfolding homeomorphism”, which is obtained by trying to solve the alternating Beltrami equation

$$\begin{cases} \frac{\partial}{\partial \bar{z}} h_n = 0 & \text{in } S_n^+ \\ \frac{\partial}{\partial z} h_n = 0 & \text{in } S_n^- \end{cases}$$

with enforcing the shape constraints of Ω_n . This will be provided by the linear Beltrami solver for rectangular target domains. The next mapping g_{n+1} is constructed based on the updated domain with its singular set configuration

$$\Sigma_n = h_n \circ g_n(\Sigma_{n-1}).$$

We wish that as $n \rightarrow +\infty$, g_n converges to a generalized conformal mapping $f : \Omega \rightarrow S$, and the composition

$$h_n \circ g_n := \psi_n$$

converges to id_Ω , while

$$\psi_n \circ \cdots \circ \psi_2 \circ \psi_1 := \varphi_n$$

converges to a quasiconformal mapping that transforms the initial singular set configuration to a desirable one. This is shown schematically in the following diagram (to add some experimental results)

$$(11) \quad \begin{array}{ccccccc} \Omega_{\Sigma_0} & \xrightarrow{\psi_1} & \Omega_{\Sigma_1} & \xrightarrow{\psi_2} & \Omega_{\Sigma_2} & \xrightarrow{\psi_3} & \cdots \Omega_{\Sigma_{n-1}} \xrightarrow{\psi_n} \Omega_{\Sigma_n} \cdots \\ \downarrow g_1 & \nearrow h_1 & \downarrow g_2 & \nearrow h_2 & \downarrow g_3 & \nearrow h_3 & \downarrow g_n \nearrow h_n \\ S_1 & & S_2 & & S_3 & & S_n \end{array}$$

In each step we enforce the available data S_{vis} by the mapping g_n , and by h_n we enforce the known boundary shape of Ω , hence the name reinforcement iteration.

3.4. The optimisation problem and the algorithm. Following the notations as above, let Ω_Σ^+ , Ω_Σ^- be the two disjoint open sets in Ω specified by some singular set configuration Σ as the orientation preserving part and the reversing part, respectively. The original objective is to find a folding homeomorphism f such that

$$\arg \min_{f, \Sigma} \int_{\Omega_\Sigma^+} \left\| \frac{\partial f}{\partial \bar{z}} \right\|^2 + \int_{\Omega_\Sigma^-} \left\| \frac{\partial f}{\partial z} \right\|^2,$$

subject to the constraint

$$f|_{\Omega_{\text{vis}}} : \Omega_{\text{vis}} \rightarrow S_{\text{vis}}.$$

Note that Σ is a variable in the minimization problem. This formulation as it stands seems very hard to implement. The discussion in the last section leads to the following relaxation, which depends on the initial singular set configuration Σ_0 :

$$(12) \quad \arg \min_{f, \varphi} \left(E(f, \varphi) := \int_{\Omega_{\Sigma_0}^+} \left\| \frac{\partial f}{\partial \bar{z}} \circ \varphi \right\|^2 + \int_{\Omega_{\Sigma_0}^-} \left\| \frac{\partial f}{\partial z} \circ \varphi \right\|^2 \right)$$

subject to the constraints

$$f|_{\Omega_{\text{vis}}} : \Omega_{\text{vis}} \rightarrow S_{\text{vis}},$$

where the argument f , defined on Ω , ranges in the set “folded homeomorphisms”, and $\varphi : \Omega \rightarrow \Omega$ ranges in the set of quasiconformal homeomorphisms. Sometimes it is also convenient to express the quantities such as $\int_{\Omega_{\Sigma_0}^+} \left\| \frac{\partial f}{\partial \bar{z}} \circ \varphi \right\|^2$ to be $\int_{\Omega_{\Sigma_\varphi}^+} \left\| \frac{\partial f}{\partial \bar{z}} \right\|^2$, where $\Omega_{\Sigma_\varphi} = \varphi(\Omega_{\Sigma_0})$. Note that if φ gives the “correct” singular set configuration, then the above energy vanishes for f that is generalized conformal.

Our iteration algorithm in the last section is then to find such mappings φ and f . The basic steps are constructions of the mappings g_n and h_n , which we now turn to.

3.5. Construction of g_n . Given the updated domain $\Omega_{\Sigma_{\varphi_{n-1}}} = \varphi_{n-1}(\Omega_{\Sigma_0})$, we obtain the S_{vis} -enforced mapping g by solving a alternating Beltrami equations subject to the constraints

$$g|_{\Omega_{\text{vis}}} : \Omega_{\text{vis}} \rightarrow S_{\text{vis}}.$$

Since we mainly care about the partial boundary and singular data enforcement here, the values of the beltrami coefficients does not matter so much. But unless there is some good reason, it's better in practice not to introduce artificial distortion, hence we often set the Beltrami coefficients to be 0 and ∞ , corresponding the orientation preserving and reversing regions, respectively.

In terms of triangular meshes, suppose the domain trangular mesh is \mathcal{D}_{n-1} , with \mathcal{D}_{n-1}^+ , \mathcal{D}_{n-1}^- corresponds to Ω_{n-1}^+ and Ω_{n-1}^- , respectively; S_{vis} is realized as certain constraint C_{vis} . Then the folded surfaced is obtained by

$$\mathcal{S}_{g_n} = \text{LSQC}(\mathcal{D}_{n-1}, \{\mu_T\}_{\mathcal{D}_{n-1}}, C_{\text{vis}})$$

where

$$\mu_T = \begin{cases} 0 & \text{if } T \in \mathcal{D}_{n-1}^+ \\ \infty & \text{if } T \in \mathcal{D}_{n-1}^- \end{cases}.$$

3.6. Construction of h_n . Given the folded surface constructed from the last step $S_n = g_n(\Omega_{n-1})$, the unfolding map $h_n : S_n \rightarrow \Omega_n$ is found by solving the minimization problem

$$\arg \min_h \left(\int_{S_n^+} \left\| \frac{\partial h}{\partial \bar{z}} \right\|^2 + \int_{S_n^-} \left\| \frac{\partial h}{\partial z} \right\|^2 \right)$$

subject to the shape constraints

$$h|_{\partial S_n} : \partial S_n \rightarrow \partial \Omega.$$

φ_n is then updated by $\varphi_n = h_n \circ g_n$. In terms of triangular meshes, suppose the folded surface mesh is \mathcal{S}_n , with \mathcal{S}_n^+ , \mathcal{S}_n^- corresponds to S_n^+ and S_n^- , respectively; $\partial \Omega$ is realized as certain constraint $C_{\partial \Omega}$. Then the above minimization can be solved by

$$\mathcal{D}_{\Sigma_n} = \text{LSQC}(\mathcal{S}_n, \{\mu_T\}_{\mathcal{S}_n}, C_{\partial \Omega})$$

where

$$\mu_T = \begin{cases} 0 & \text{if } T \in \mathcal{S}_n^+ \\ \infty & \text{if } T \in \mathcal{S}_n^- \end{cases}.$$

The overall algorithm is thus summarized as Algorithm 1.

Algorithm 1 Reinforcement Iteration

Initialize Σ_0 , $\epsilon > 0$, itermax > 0 ,
Construct g_1 , h_1 ; compute $\varphi_1 = u_1 \circ f_1$.
Evaluate $E(g_1, \varphi_1)$, $E(g_0, \varphi_0) = 0$, $n = 1$.
while $|E(g_n, \varphi_n) - E(g_{n-1}, \varphi_{n-1})| > \epsilon$ and $n < \text{itermax}$. **do**
 Provided φ_{n-1} , construct g_n , h_n .
 Compute $\varphi_n = h_n \circ g_n \circ \varphi_{n-1}$.
 Evaluate $E(g_n, \varphi_n)$.
end while

One might wish to compare this algorithm with the adjoint method that is commonly used in PDE constrained optimization. Here, the method would proceed as a gradient descent on the generalized conformal distortion

$$\arg \min_{f, \Sigma} \int_{\Omega_\Sigma^+} \left\| \frac{\partial f}{\partial \bar{z}} \right\|^2 + \int_{\Omega_\Sigma^-} \left\| \frac{\partial f}{\partial z} \right\|^2$$

subject to the constraints. More generally in the discrete case, the descent step can be on the coordinates of possibly a subset of the domain vertices. For the sake of discussion let us assume this subset is the singular set Σ and the coordinates of its elements are denoted by p , and we write x to be the vertex coordinates of the folding map f . The optimization problem can be written as

$$\arg \min_{x, p} F(p, x(p)) \quad \text{subject to} \quad G(p, x(p)) = 0.$$

where $G(p, x(p)) = M'(p)x(p) - b = 0$ expresses the requirement that $x(p)$ should be the solution of the alternating Beltrami equation with enforced constraints.

To minimize $F(p, x(p))$, we first notice that

$$d_p F(p, x(p)) = \partial_p F(p, x(p)) + \partial_x F(p, x(p)) \partial_p x(p)$$

where d_p denotes the total derivative and ∂_p denotes the partial derivative. Since we also have the constraint $G(p, x(p)) = 0$, we consider the Lagrangian L :

$$L(p, x(p), \lambda) = F(p, x(p)) + \lambda^T G(p, x(p)).$$

Thanks to the constraint $G(p, x(p)) = 0$, we have

$$F(p, x(p)) = L(p, x(p), \lambda) \quad \text{for all } \lambda$$

Therefore, we have

$$\begin{aligned} d_p L &= d_p F = \partial_p F(p, x(p)) + \partial_x F(p, x(p)) \partial_p x(p) + \partial_p G(p, x(p)) \lambda + \partial_p x \partial_x G(p, x(p)) \lambda \\ &= \partial_p F(p, x(p)) + \partial_p G(p, x(p)) \lambda + \partial_p x (\partial_x F + \partial_x G \lambda) \end{aligned}$$

As λ can be chosen arbitrary, to eliminate the difficulty of evaluating $\partial_p x$ (intuitively, this is the gradient of the folding map subject to the change of the singular set), we can choose $\lambda \equiv \lambda_*$ such that

$$\partial_x F + \partial_x G \lambda_* = 0.$$

Then we have

$$d_p F = \partial_p F + \partial_p G \lambda_*.$$

More precisely, we choose λ_* such that $\lambda_* = (\partial_x G)^{-1} \partial_x F$ assuming that $(\partial_x G)^{-1}$ exists.

Once we obtain λ_* , the descent direction can be obtained to update p_n , that is

$$p_{n+1} = p_n - \gamma_n d_p F(p, x(p)),$$

where γ_n is some step size for gradient descent. Rewriting the above update, we have

$$p_{n+1} = p_n - \gamma_n [\partial_p F(p, x) + \partial_p G(p, x) (\partial_x G(p, x))^{-1} \partial_x F].$$

So basically there are two separate terms to update p_n .

Now the term $\partial_p F(p, x)$ can be interpreted as the perturbation direction for the singular set vertices. This can be understood as similar to the h_n construction step in the n -th iteration of our algorithm. For the other term, notice that $\partial_x G(p, x) = M'(p)$, and we can view $\partial_x F$ as the change of Ω_{vis} by the previous update h_n , interpreted as the amount of “extra charge” the constraints imply. Thus $(\partial_x G(p, x))^{-1} \partial_x F = M'(p)^{-1} \partial_x F = \delta x$. Multiplying it by $\partial_p G$ then gives us the direction of the change of p provided by δx subject to the constraint $G(p, x(p)) = 0$. Therefore, this update can be compared to the construction of g_n in our algorithm. However, computing the partial derivatives $\partial_p F(p, x)$ and $\partial_p G$ is difficult and may not be satisfactory since the optimal set of “control points” p may be hard to choose *a priori*. In addition, the choice of the step size γ_n is again challenging as it is difficult to estimate the scale of the gradient.

4. Further discussion and experimental results. Several remarks are in order. First, finding the critical point for the generalized quasiconformal energy is an easy saddle point problem by solving linear equations. We can reconcile it with the minimization problem in the construction h_n by noting that the two are equivalent provided the folded and unfolded part of h_n matched up, which is of course part of the continuity assumption about h_n .

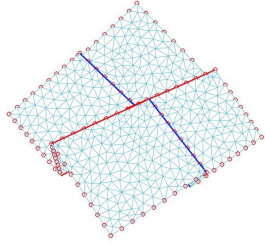
Second, we notice that the desirable domain x^* and its folded counterpart y^* are fixed points of our iteration algorithm, which can be written as $x^* = \mathcal{F}(x^*)$, where \mathcal{F} is the iteration mapping in operator form. Note that \mathcal{F} depends on its argument x in a very non-linear way because of the auxiliary variable y we introduced, whose computation requires the cotangent matrix associated to x . The convergence of fixed point iteration is well studied in the literature [5]. For example, the convergence will be implied by the α -averaged property of \mathcal{F} . As we can notice in Figure 3, as well as in many other experiments we have done, the distortion of many of the interior mesh triangles can barely be noticed in the later phase of the iteration. And the meshes are also well conditioned. So it is reasonable to assume at least that the mapping in the later phase of the iteration to have such averagedness property.

We implemented the described reinforcement iteration algorithm for a doubly folded surface, as illustrated in Figure 3. The folded surface and its unfolded counterpart, as shown in Figure 3a and 3b, are generated according to a real folded paper and its unfolded counterpart. In Figure 3c it is our initialized domain Ω_{Σ_0} . In 3a and 3c, the red circles mark the corresponding constraint points to the visible partial singular set and boundary data. Our algorithm works similarly well with other examples as well. This shows the robustness of our algorithm.

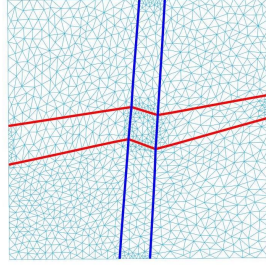
In the next three rows of Figure 3 we show the iteration results at the first iteration, 50-th iteration and 200-th iteration. We can observe the curly folding lines in the first iteration in Figure 3e and 3f. This is due to the incomplete data and the incompatible initialized domain. In the subsequent iterations we saw significant improvement over the rigidity of the folding. In practice we also found that if we explicitly regularize the singular lines by e.g. projecting them onto a Euclidean geodesic, and then restart the iteration, the convergence will be improved in particular for the multiply folded cases.

Observe also that in the limit, as in Figure 3l, the singular set configuration is in not exactly the same with that of the true unfolded surface. This can be explained by the existence multiple admissible solutions to this problem. For example, another admissible solution may be obtained by some different initialization. This is of course expected.

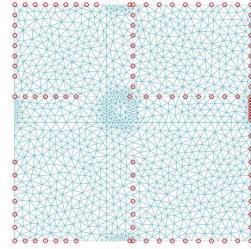
In Figure 4, we plot a log-log diagram for the energy $E(g_k, \varphi_k)$ that we aim to minimize for the same example, with “log(Loss)” legend name. We can observe that the convergence rate approaches $O(1/N)$ in the mid-stage of the iteration. That the energy decreases slightly slower in the later phase can be explained by our observation from the iterations that only a few points are adjusted while the singular set configuration is still away from flat-foldability. These adjusted points are mainly near the cusp points. This fact can be observed from Figure 3f and 3i. The convergence somehow becomes faster in the late phase of the iteration, illustrating the non-linear nature of the iteration.



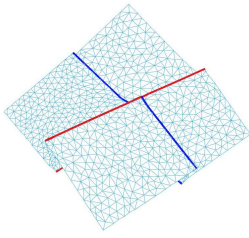
(a) Folded surface with occlusion.



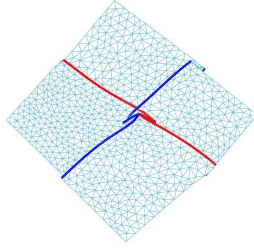
(b) True unfolded surface.



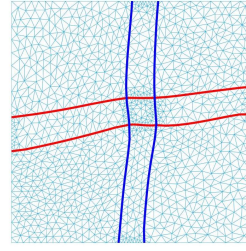
(c) Initialised domain with partial data.



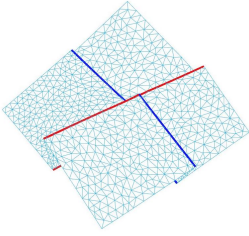
(d) Iter = 1: Frontside of registered fold.



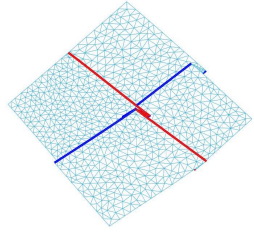
(e) Iter = 1: Backside of registered fold.



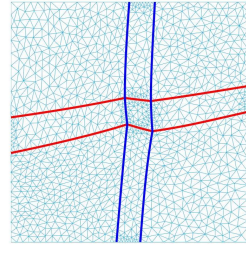
(f) Iter = 1: Unfolded surface.



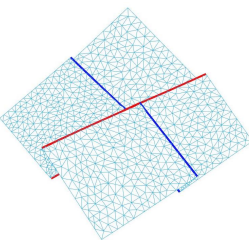
(g) Iter = 50: Frontside of registered fold.



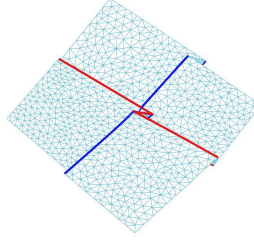
(h) Iter = 50: Backside of registered fold.



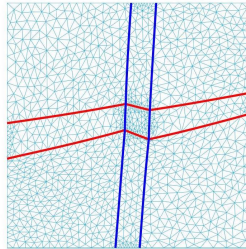
(i) Iter = 50: Unfolded surface.



(j) Iter = 200: Frontside of registered fold.



(k) Iter = 200: Backside of registered fold.



(l) Iter = 200: Unfolded surface.

Fig. 3: Iteration results for the doubly folded surface.

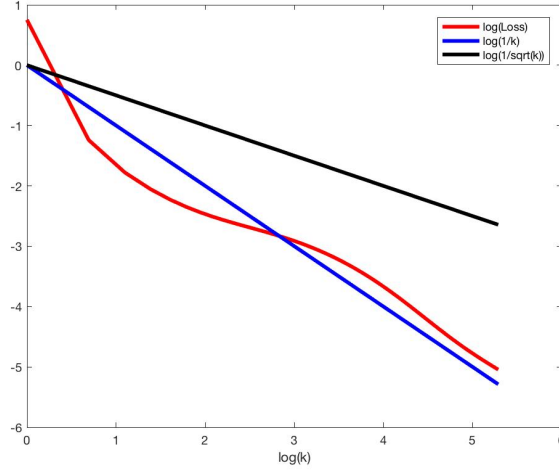


Fig. 4: Convergence plot for the doubly folded surface



(a) User chosen folding region (b) Fold-like texture generated

Fig. 5: Fold-texture generation with user selection folding region

5. Applications.

5.1. Almost rigid folding with application to fold-texture generation, fold sculpting and fold inpainting. As one of the immediate applications, we can consider a folding transformation on the texture space to create synthetic fold-like textures, prior to applying the texture map. This can be cheap to do if high quality physical simulation and rendering is not available. In Figure 5 we explore such a possibility of user-designed fold-like texture generation. For the purpose of visual illustration we put the texture image in a white background. The user then can designate a region which is meant to be folded, as shown in Figure 5a. Then the fold-like texture can be obtained by solving a single alternating Beltrami equation followed by a planar texture mapping, which is very fast. The resulting texture exhibits cloth-like folding pattern, as is shown in Figure 5b. Note that the folding lines are not necessarily Euclidean geodesics, and the rigidity of the original texture is still well-preserved.



Fig. 6: Folding effect texturing on a 3D model. Note that the mesh model is not deformed.

One of the fundamental step in texturing a 3D surface is to find the parameterization (or the texture map) $f : S \rightarrow \Omega \in \mathbb{R}^2$. In particular, UV mapping is one of the major type of parameterization techniques in various software packages, which works well if the 3D model is created from polygon meshes. The above technique can be very useful in the interactive user design, where user directly operates on the target mesh, and the input is transformed to the texture domain via the UV-map, to create desirable fold-like texture on the target mesh. It is also possible to incorporate proper shading effect on the transformed texture directly, making the texture look more realistic. We have implemented such a fold-like texturing method using a 3D T-shirt model, shown in Figure 6b. Note that the mesh is not deformed at all.

We can also apply the folding technique directly to the 3D meshes, as an application we would like to call *fold sculpting*. To illustrate this, we select a patch from the T-shirt model, as shown in Figure 7a. We applied the folding operation to a suitable parametrization of the patch, which can be obtained easily via e.g. projection or a least square conformal parametrization [18], and then glue it back to the T-shirt model. Note that our algorithm produces sharp edges. This can be mitigated by some standard smoothing operation in various mesh editing software. Figure 8 and 9 show the results after appropriate smoothing, where we used the software Maya³ to the smoothing and rendering tasks. Note that the such folding is not easily obtained by pure handcraft, since one part of the cloth actually folds over and covers some other part of the cloth.

The technique can also be applied after the acquisition of a folded surface using laser scans, where the folded part introduces self-occlusions and the folding is usually diminished or destroyed after applying the watertight operation. To preserve the folding details from the scans directly, we can mark the folding part that we want to preserve in the raw acquisition. By taking a patch like before and mapping it into the plane, we can solve a proper alternating Beltrami equation to obtain the desired folding effect. The folded patch can then be mapped back to the raw acquisition. To

³A software of the Autodesk Inc. See <https://www.autodesk.com.hk/products/maya/overview>. The results are generated under the student license obtained by the first author.

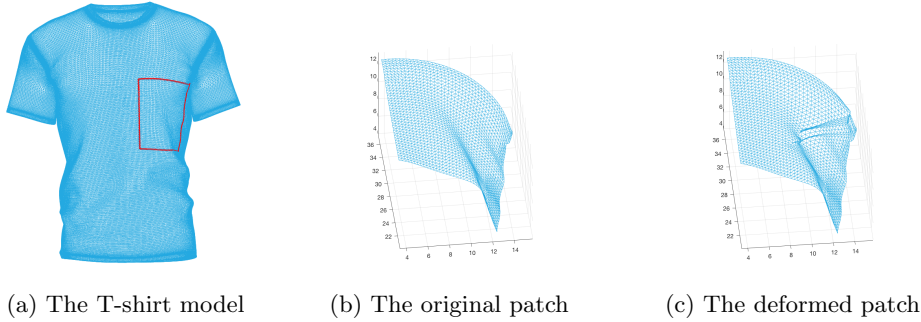


Fig. 7: Patch-wise fold sculpting: the region inside the red contour is the patch selected, appropriate alternating Beltrami equation is then solved in the patch domain to obtain the desired folding effect.

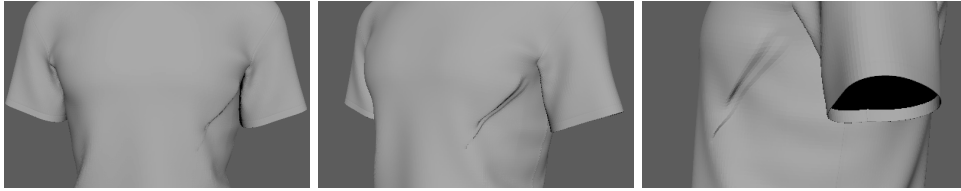


Fig. 8: Results of fold sculpting on the T-shirt model after appropriate smoothing: two short folds are sculpted on the right.

illustrate this, we have done a synthetic experiment using the above approach. We begin with an incomplete acquisition of a shirt model, such as the one on the left in Figure 11. As demonstrated in Figure 10, the patch with holes is first map to the plane and subsequently filled. A suitable folding operation is then applied to the patch to produce a plausible fold geometry given the acquisition data. The reconstruction is shown in Figure 11 on the right, again after appropriate smoothing.

5.2. Self-occlusion reasoning of flat-foldable surfaces and its application to restoration of folded images. As is described in Section 3.2, given a single perspective of a folded surface, for example, shown in figure 12, we can use the proposed reinforcement iteration to unfold the surface, thus enabling us to identify the self-occluded region in the unfolded domains, shown in Figure 13.

Meanwhile, various methods for high-level editing of digital photographs and video have been proposed. For example, image retargeting algorithms are proposed for resizing image while preserving the aspect ratio of important contents in the images [27]; The procedure of finding one-one correspondence between images is called image registrations, which is one of the fundamental steps for image comparison and statistical analysis of image data [17, 19]; image completion techniques are also proposed to allow user to erase unwanted portions in the image and automatically refill the missing parts with tenable synthesis texture. In particular, the process of synthesizing these artificial image portion is sometimes called *image inpainting*. In this example, we demonstrate the improvement of inpainting result brought about by considering

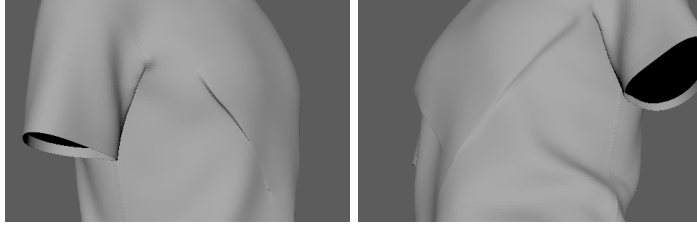


Fig. 9: Results of fold sculpting on the T-shirt model after appropriate smoothing: two long folds are sculpted on the left and right.

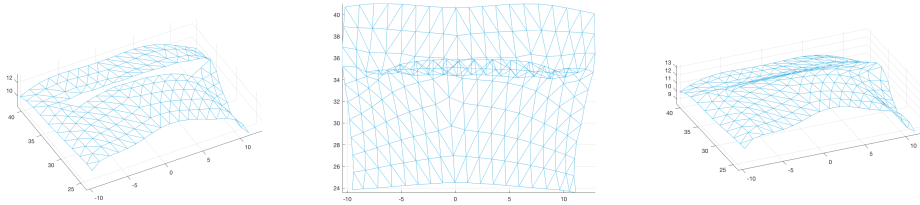


Fig. 10: Patch-wise fold inpainting: from the raw acquisition of a self-occluded surface, we map the occluded, holed surface to the plane and fill the hole; we then apply a suitable folding operation to reproduce the fold that was not captured during acquisition.

the partial geometric information of the image via our unfolding procedure.

Given a folded image, the task of restoring the image involves unfolding the image and inpainting the missing parts beneath the folded region. The performance of the final restoration results obviously depends on the realization of the texture synthesis. However, it is worth noting that the unfolding result may also drastically affects the inpainting result since many inpainting methods such as the diffusion-based [3, 26], exemplar-based [7, 1, 2] assume the full knowledge of the computational domain (i.e., the image domain). To alleviate the difficulty arose from the incomplete knowledge of the image domain, we can employ the proposed unfolding algorithm to retrieve the geometric information of the folded subdomain with the given partial geometric information. Once we restore the intrinsic image domain consistent with the partial geometric information, well-developed inpainting techniques can then be employed correctly and provides satisfactory inpainting results.

Figure 14 shows the result for the 1-folded example. The unfolding is trivial in a sense, but here we want to use it to illustrate the typical procedure of a folded-image restoration. The same procedure applies to all kinds of folds alike. In any case, we assume to have the partial boundary and singular set data (i.e., the folding edges and the boundaries) available from the folded images. Our goal is to recover the folded image 12a by using the proposed unfolding technique and some well-established inpainting algorithms. At the beginning of our algorithm, an initialization Σ_0 is constructed by simply using the partial boundary and singular set data. By the proposed Algorithm 1, we can successfully reconstruct the folding map based on the reinforcement iterations, which are shown in 14b. With the folding map, we can obtain the occluded

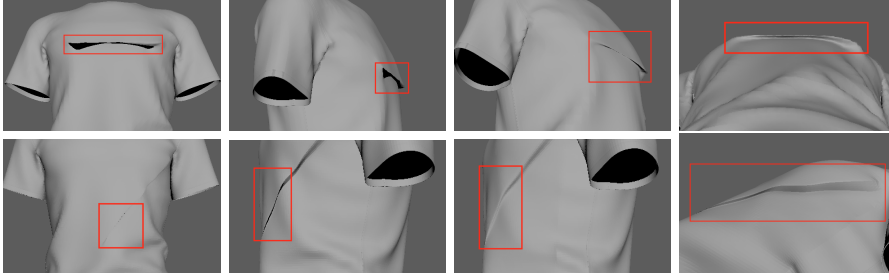


Fig. 11: Results of fold inpainting: the first row and second row are two examples of the technique. For each row, the two on the left are the surface with holes from acquisition due to self occlusion. The results of inpainting are the two on the right. The corresponding holed and inpainted regions are highlighted inside the red boxes.



Fig. 12: 1-folded, 2-folded, 3-folded and 4-folded examples

region and carry out the inpainting procedure. Notice that the unfolded mesh in 14b highly resembles to the ground truth (see 14a). With such unfolded domain, we can accurately approximate the masked region and apply the patch-matching based inpainting algorithm to recover the image. The corresponding parametrized folding surfaces are shown in figure 14c. The image can then be mapped from the folded surface back to the domain complementary to the occluded region. Here, as is common the case, due to the size of masked region generated from the fold of the image, we choose the patch-matching based algorithm for image inpainting. In particular, we employ the algorithm⁴ proposed by Daisy et. al. [7] in this example. The result is shown in 14d. For comparison, the original image together with the overlapping mask (drawn as a half-transparent domain) is shown in Figure 13a.

To illustrate the adaptability of our proposed algorithm in more complicated folded surface, we now consider correspondingly, a 2-, 3- and 4-folded examples, as shown in Figure 12. There is a 2-folded painting "The Sower" by Vincent van Gogh; a 3-folded "building" image, and a 4-folded "flower" image.

⁴The algorithm is available as an plugin for the open source GIMP2 software. The software is available at <https://www.gimp.org/>.

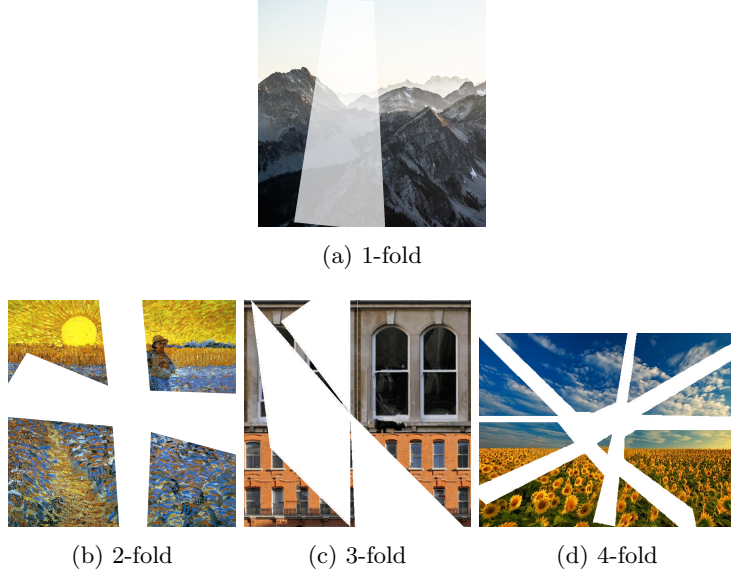


Fig. 13: Occluded regions of various folded paper examples

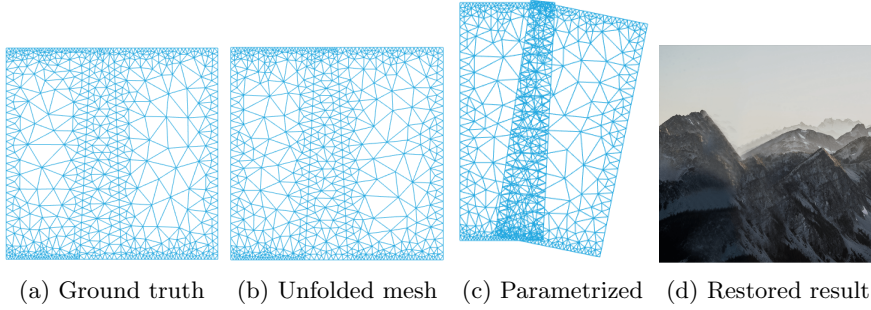


Fig. 14: Unfolding and restoring result of a 1-folded image.

Similarly, to approximate the original images with the given folded data, we first have to unfold these surfaces using the proposed algorithm. Unlike the trivial 1-fold example illustrate above (which may be simply get unfolded even without the use of Algorithm 1), the folding order also takes part in this unfolding problem since different orders of folding produce different folded images. When the folding number is large, obtaining the ordering of the folds from the given data is difficult. However, using the Algorithm 1, this folding order can be obtained implicitly. In other words, the unfolding procedure using Algorithm 1 is fully automatic. Figure 15 shows the unfolding and the corresponding inpainting results. The leftmost column shows the folded meshes corresponding to some unidentified rectangular meshes. With only partial boundary conditions and singular set data, unfolding these surfaces are highly ill-posed. But using our proposed algorithm, we successfully obtained the unfolding

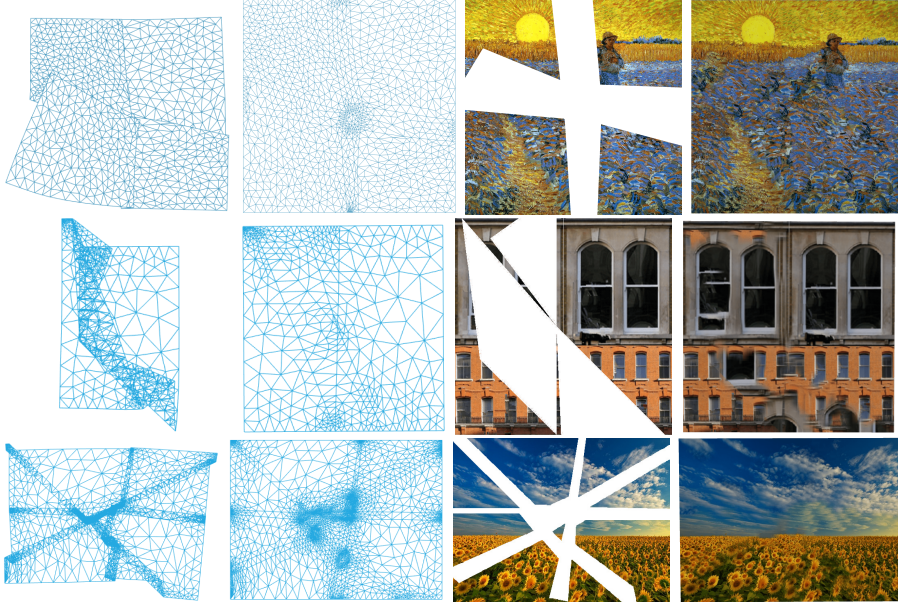


Fig. 15: Unfolding and inpainting result for the 2-fold (first row), 3-fold (second row) and 4-fold (last row) examples. Leftmost column shows the folded meshes representing the domain of the images. The unfolded results are shown in the middle-left column and the recovered occluded domains are shown in the middle-right columns. The overall recovery results are shown in the rightmost column.

surfaces (the middle-left column). Notice that by regularizing the generalized Beltrami coefficient, Algorithm 1 converges to unfolded regular meshes, where unnatural curvy edges are not presented. With these unfolded meshes, we can recover the occluded regions due to the foldings (See the middle-right column) and therefore inpainting algorithms can be employed as usual. The overall recovered images are shown in the rightmost column of Figure 15.

6. Conclusion. We have proposed a novel way of studying and modeling the folding phenomena of surfaces using alternating Beltrami equations. The numerical scheme is proposed to overcome the known issues of the previous method, by taking into account of the coupled nature of the two coordinate functions of the solution. The resulting method works for fewer constraints, and has a nice geometric interpretation. More importantly, it allows us to formulate and solve the inverse problem of inferring and parametrizing flat-foldable surfaces with observed partial data. We have proposed to use the "reinforcement iteration" algorithm in order to solve the associated optimization problem, which has shown empirical convergence over various examples. Various applications are given, including fold sculpting, fold-like texture generation, as well as self-occlusion reasoning. Many more possible applications in manufacturing, animation and modelling shall be explored in the future. At the same time, the understanding of non-rigid folding is still largely incomplete and many more interesting examples and applications are waiting to be discovered.

Acknowledgments. The authors would like to thank Mr. Leung Liu Yusan and Dr. Emil Saucan for the useful discussions in the early stage of this work. The examples meshes are generated by the software Triangle [22].

REFERENCES

- [1] C. BARNES, E. SHECHTMAN, A. FINKELSTEIN, AND D. B. GOLDMAN, *Patchmatch: A randomized correspondence algorithm for structural image editing*, ACM Trans. Graph., 28 (2009), pp. 24–1.
- [2] C. BARNES, E. SHECHTMAN, D. B. GOLDMAN, AND A. FINKELSTEIN, *The generalized patchmatch correspondence algorithm*, in European Conference on Computer Vision, Springer, 2010, pp. 29–43.
- [3] M. BERTALMIO, G. SAPIRO, V. CASELLES, AND C. BALLESTER, *Image inpainting*, in Proceedings of the 27th annual conference on Computer graphics and interactive techniques, ACM Press/Addison-Wesley Publishing Co., 2000, pp. 417–424.
- [4] P. T. CHOI, K. C. LAM, AND L. M. LUI, *Flash: Fast landmark aligned spherical harmonic parameterization for genus-0 closed brain surfaces*, SIAM Journal on Imaging Sciences, 8 (2015), pp. 67–94.
- [5] P. L. COMBETTES, *Solving monotone inclusions via compositions of nonexpansive averaged operators*, Optimization, 53 (2004), pp. 475–504.
- [6] B. DACOROGNA, P. MARCELLINI, AND E. PAOLINI, *Lipschitz-continuous local isometric immersions: rigid maps and origami*, Journal de mathématiques pures et appliquées, 90 (2008), pp. 66–81.
- [7] M. DAISY, D. TSCHUMPERLÉ, AND O. LÉZORAY, *A fast spatial patch blending algorithm for artefact reduction in pattern-based image inpainting*, in SIGGRAPH Asia 2013 Technical Briefs, ACM, 2013, p. 8.
- [8] E. D. DEMAINE AND T. TACHI, *Origamizer: A practical algorithm for folding any polyhedron*, in LIPIcs-Leibniz International Proceedings in Informatics, vol. 77, Schloss Dagstuhl-Leibniz-Zentrum fuer Informatik, 2017.
- [9] M. DESBRUN, M. MEYER, AND P. ALLIEZ, *Intrinsic parameterizations of surface meshes*, in Computer graphics forum, vol. 21, Wiley Online Library, 2002, pp. 209–218.
- [10] L. H. DUDTE, E. VOUGA, T. TACHI, AND L. MAHADEVAN, *Programming curvature using origami tessellations*, Nature materials, 15 (2016), pp. 583–588.
- [11] X. GU, Y. WANG, T. F. CHAN, P. M. THOMPSON, AND S.-T. YAU, *Genus zero surface conformal mapping and its application to brain surface mapping*, IEEE Transactions on Medical Imaging, 23 (2004), pp. 949–958.
- [12] X. D. GU, R. GUO, F. LUO, AND W. ZENG, *Discrete laplace-beltrami operator determines discrete riemannian metric*, arXiv preprint arXiv:1010.4070, (2010).
- [13] V. GUTLYANSKII, V. RYAZANOV, U. SREBRO, AND E. YAKUBOV, *Alternating beltrami equation, The Beltrami Equation*, (2012), pp. 183–208.
- [14] T. IGARASHI, T. MOSCOVICH, AND J. F. HUGHES, *As-rigid-as-possible shape manipulation*, in ACM transactions on Graphics (TOG), vol. 24, ACM, 2005, pp. 1134–1141.
- [15] M. KILIAN, S. FLÖRY, Z. CHEN, N. J. MITRA, A. SHEFFER, AND H. POTTSMANN, *Curved folding*, in ACM Transactions on Graphics (TOG), vol. 27, ACM, 2008, p. 75.
- [16] T.-H. KWOK, C. C. WANG, D. DENG, Y. ZHANG, AND Y. CHEN, *Four-dimensional printing for freeform surfaces: design optimization of origami and kirigami structures*, Journal of Mechanical Design, 137 (2015), p. 111413.
- [17] K. C. LAM AND L. M. LUI, *Landmark-and intensity-based registration with large deformations via quasi-conformal maps*, SIAM Journal on Imaging Sciences, 7 (2014), pp. 2364–2392.
- [18] B. LÉVY, S. PETITJEAN, N. RAY, AND J. MAILLOT, *Least squares conformal maps for automatic texture atlas generation*, in ACM transactions on graphics (TOG), vol. 21, ACM, 2002, pp. 362–371.
- [19] L. M. LUI, K. C. LAM, S.-T. YAU, AND X. GU, *Teichmüller mapping (t-map) and its applications to landmark matching registration*, SIAM Journal on Imaging Sciences, 7 (2014), pp. 391–426.
- [20] L. M. LUI, T. W. WONG, W. ZENG, X. GU, P. M. THOMPSON, T. F. CHAN, AND S.-T. YAU, *Optimization of surface registrations using beltrami holomorphic flow*, Journal of scientific computing, 50 (2012), pp. 557–585.
- [21] U. PINKALL AND K. POLTHIER, *Computing discrete minimal surfaces and their conjugates*, Experimental mathematics, 2 (1993), pp. 15–36.
- [22] J. R. SHEWCHUK, *Triangle: Engineering a 2d quality mesh generator and delaunay triangulation*

- lator*, in Applied computational geometry towards geometric engineering, Springer, 1996, pp. 203–222.
- [23] O. SORKINE AND M. ALEXA, *As-rigid-as-possible surface modeling*, in Symposium on Geometry processing, vol. 4, 2007.
 - [24] O. SORKINE, D. COHEN-OR, Y. LIPMAN, M. ALEXA, C. RÖSSL, AND H.-P. SEIDEL, *Laplacian surface editing*, in Proceedings of the 2004 Eurographics/ACM SIGGRAPH symposium on Geometry processing, ACM, 2004, pp. 175–184.
 - [25] U. SREBRO AND E. YAKUBOV, *Branched folded maps and alternating beltrami equations*, Journal d’analyse mathématique, 70 (1996), pp. 65–90.
 - [26] D. TSCHUMPERLE AND R. DERICHE, *Vector-valued image regularization with pdes: A common framework for different applications*, IEEE transactions on pattern analysis and machine intelligence, 27 (2005), pp. 506–517.
 - [27] C. P. YUNG, G. P.-T. CHOI, K. CHEN, AND L. M. LUI, *Trim: Triangulating images for efficient registration*, arXiv preprint arXiv:1605.06215, (2016).
 - [28] R. ZAYER, C. ROSSL, AND H.-P. SEIDEL, *Discrete tensorial quasi-harmonic maps*, in Shape Modeling and Applications, 2005 International Conference, IEEE, 2005, pp. 276–285.
 - [29] L. ZHU, T. IGARASHI, AND J. MITANI, *Soft folding*, in Computer Graphics Forum, vol. 32, Wiley Online Library, 2013, pp. 167–176.